

# Exact analysis of a practical quantum repeater architecture with noisy elements

Saikat Guha, Hari Krovi, Christopher A. Fuchs, Zachary Dutton

*Quantum Information Processing group, Raytheon BBN Technologies, 10 Moulton Street, Cambridge, MA USA 02138*

Joshua A. Slater<sup>†</sup>, Christoph Simon, Wolfgang Tittel

*Institute for Quantum Science and Technology, and Department of Physics, University of Calgary, Alberta, T2N 1N4*

<sup>†</sup>*Vienna center for quantum science and technology (VCQ),  
Faculty of Physics, University of Vienna, 1090 Vienna, Austria*

We analyze a long-distance entanglement-based quantum key distribution (QKD) architecture that uses a chain of multi-mode atomic-memory-based quantum repeaters employing linear-optic Bell-state measurements, frequency-multiplexed broadband sources of entanglement, and classical-only error correction, i.e., no quantum purification—which typically is the hardest step in conventional repeater protocols. We find an exact expression for the secret-key rate, and an analytical characterization of how errors propagate through the repeater links in the chain, as a function of the loss and noise parameters of the memories, channel, and detectors. We assume the sources to have zero two-pair emission probability, i.e.,  $p(2) = 0$ , to develop the exact analytical results. We then present numerical results that suggest that the aforesaid error-propagation scaling also holds with non-zero two-pair-emission rates, with a  $p(2)$ -dependent correction to the constant term in the scaling law. We show that our repeater architecture achieves a rate-loss scaling that far surpasses the recently-found fundamental upper limit to the rate-loss scaling achievable by *any* QKD protocol without quantum repeaters, given the same pulse repetition rate and frequency-bandwidth. We show how various source and detector non-idealities affect the rate-loss envelope, and that the effect of the principle detriments can be separately assessed. Aside from the QKD rate calculations, we also exactly characterize the evolution of the end-to-end entangled quantum state through the repeater chain, which could be useful to analyze other distributed quantum information protocols that require establishing long-distance entanglement.

Shared entanglement underlies many quantum information protocols such as quantum key distribution (QKD) [1], teleportation [2] and dense coding [3], and is a fundamental information resource that can boost reliable classical and quantum communication rates over noisy quantum channels [4, 5]. Optical photons are arguably the only candidate for distributing entanglement across long distances. They however are susceptible to loss and noise in the channel, which is the bane of practical realizations of long-distance quantum communication. The maximum entanglement-generation rate over a lossy optical channel with no classical-communication assistance is zero when the total loss exceeds 3 dB [6]. With two-way classical-communication assistance, the rates achievable for entanglement generation, as well as those for reliable quantum communication and secret-key generation (i.e., QKD) over a lossy optical channel must decay linearly with the channel’s transmittance (i.e., exponentially with optical fiber length), regardless of the specific protocol used, for loss exceeding  $\sim 5$  dB [7], while the rate plunges to zero at a maximum loss threshold that is determined by the excess noise in the channel and detectors. In order to generate entanglement over long distances at high rates, intermediate nodes equipped with quantum processing power must be interspersed along the lossy channel. *Quantum repeaters* are one example of such nodes that can help circumvent the aforesaid linear rate-transmittance fall-off of the unassisted lossy channel. However, not all quantum devices can serve as effective intermediate nodes. For example, quantum-

limited phase-sensitive amplifiers inserted along the lossy channel cannot improve upon quantum communication performance over the unassisted pure-loss channel [8].

Several quantum repeater protocols have been proposed, all of which use entanglement swapping by Bell-state measurements, and quantum memories, of some form (See [9] for a recent review). The basic quantum repeater protocol probabilistically connects a string of imperfect entangled qubit pairs by using a nested entanglement swapping and purification protocol, thereby creating a single distant pair of high fidelity [10, 11]. If used for QKD, those final distant entangled pairs are measured by Alice and Bob in mutually-unbiased bases, followed by sifting, error-correction and privacy amplification over a two-way authenticated classical channel, to generate a shared secret. An alternative (the DLCZ) repeater protocol uses a chain of elementary links between pairs of atomic memories created in single-photon entangled states, followed by a distant heralded interferometric conversion of two copies of such entangled states into a two-photon entangled state. Repeater protocols usually rely on purifying multiple long-distance imperfect shared entangled pairs (into few pairs of high fidelity)—a procedure known as *entanglement distillation*. As an alternative to entanglement distillation, a forward quantum-error-correction coded architecture was proposed that generates a backbone of encoded (logical) Bell pairs and uses classical error correction during simultaneous entanglement connections at the quantum nodes [12], whose performance—in terms of its classical

communication overhead—was found to surpass that of the standard architecture [13]. In [14], a repeater architecture was proposed that uses quantum memories based on atomic ensembles and linear optics for heralded Bell state measurements [15, 16]. This protocol does not rely on purification, does not require hierarchical connection of the elementary links (i.e., multiple connections can proceed simultaneously), allows the fidelity (of the end-to-end shared entangled state) to deteriorate as the chain lengthens, and finally uses classical error correction on the correlated end-to-end measurements after the reconciliation phase, to extract shared secret keys. Despite the practical appeal of this architecture, a rigorous calculation of its performance in the presence of various loss and noise detriments, and verifying that it can fundamentally outperform a repeater-less link for QKD, has yet to be done, and is the primary purpose of this paper.

A big challenge that faces practical designs of long-distance quantum repeater architectures, is the quantitative understanding of how the shared entangled state evolves across concatenated swap operations across multiple repeater nodes, which would enable calculating the rates of various quantum communication protocols that may consume the shared entanglement. Some recent studies were done to analyze linear chains of quantum relays [19] and memory-based repeaters [14, 20], which have either used extensive numerical simulations, or proposed semi-analytic or approximate theoretical models that are not scalable.

In this paper, we present a complete analytical characterization of the evolution of the end-to-end shared-entangled state in a concatenated quantum repeater chain and evaluate its performance for QKD. We analyze the scheme proposed in [14], which uses frequency-multiplexed broadband sources of photonic entanglement, multi-mode quantum memories at repeater nodes, linear-optic Bell-state measurements, and classical error correction (but no intermediate purification). Our analysis technique can be readily applied to other repeater architectures as well. We analyze QKD using the aforesaid repeater chain, and obtain an exact expression for the secret key rate as a function of distance, number of swap stages, and various loss-and-noise parameters of the channel and detectors. We account for fiber loss, detector dark counts, detector inefficiency, multi-pair emission rates of the entanglement sources, and loss in loading (readout) into (from) quantum memories. We find a compact scaling law for how the quantum bit error rate (QBER)—the probability that Alice and Bob obtain a mismatched sifted key bit despite measuring their halves of the entangled state in the same bases—scales up with increasing number of swap levels. This analytical scaling has practical importance, since an experimentally measured QBER on a single elementary link can be used to predict the QBER (and hence the key rates) practically obtainable over a long-distance channel that is constructed with multiple elementary links made with identical imperfect devices. Our calculation

involves a detailed analysis of the Bell swap operations by modeling imperfect single-photon detectors with appropriate positive-operator-valued-measure (POVM) elements, and solving a variant of the *logistic map*, a nonlinear difference equation whose solutions are known to be chaotic in general [21]. Our calculations show that the aforesaid repeater chain, even when built using lossy and noisy devices, attains an overall rate-loss scaling for QKD that far outperforms the performance achievable by any QKD protocol that does not employ quantum repeaters. Since we calculate the exact quantum state after every swap stage, our results can be used to calculate any other quantity of interest, such as fidelity, in other applications of long-distance shared entanglement. We also simulate the repeater chain numerically, to confirm our theory. Our efficient simulation routine, which uses sparsified matrix representations of bosonic operations, enables us to go beyond sources with  $p(2) = 0$ . A non-zero two-pair probability  $p(2)$  is shown to deteriorate the rate-distance scaling for QKD, but in the following way—at any given value of  $p(2)$ , there is a maximum number  $N_{\max}(p(2)) \approx 1 + c/p(2)$  of elementary links up until which the rate-loss envelope achieved by the repeater chain remains almost identical to what is achieved by a  $p(2) = 0$  entanglement source ( $c$  is a small constant). However, as soon as  $N$  exceeds  $N_{\max}(p(2))$ , the rate crashes to zero. Even for sources with  $p(2) > 0$ , our analytical prediction of error propagation through the repeater chain is shown to hold, albeit with a  $p(2)$ -dependent modification to a pre-factor.

The paper is organized as follows. We begin with a description of the repeater architecture. We then state our main results, followed by a high-level description of the key steps of our theoretical analysis. Detailed proofs are deferred to the Appendices. Finally, we summarize our main numerical results, followed by a description of our results on the effect of source imperfections on the scaling of the secret key rate, in detail. We conclude with thoughts on open questions and future work.

## I. THE QUANTUM REPEATER ARCHITECTURE

The architecture [14] is depicted schematically in Figs. 1, 2. The total range (Alice to Bob distance) is  $L$  km of lossy fiber, divided into  $N = 2^n$  elementary links.

*The elementary links.*—At the center of each elementary link, a linear-optic Bell-state measurement (BSM) [15] acts on the halves of two pairs of maximally-entangled Bell states,  $|M^\pm\rangle \triangleq [ |10, 01\rangle \pm |01, 10\rangle ] / \sqrt{2}$ , each sent through a lossy channel of transmissivity  $\lambda = 10^{-(\alpha L/2N)/10}$ , where  $\alpha$  (in dB/km) is the fiber’s loss coefficient. The BSM at the center of each elementary link comprises a 50-50 beam-splitter followed by a pair of single-photon detectors that can spectrally-resolve between  $M$  frequency modes. We assume that the detectors are not capable of photon number resolution. The

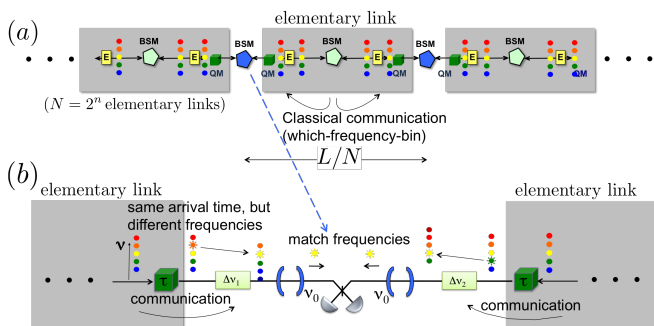


Figure 1. Schematic of quantum repeater architecture [14].

detection efficiencies and dark-click probability per mode for each detector is taken to be  $\eta_e$  and  $P_e$ , respectively. A linear-optic BSM is successful with at most 50% probability [16]. Each qubit, encoded in two temporal modes (of each frequency mode), occupies  $T_q$  seconds. The entangled photon-pair sources  $E$  at each end of the elementary link are assumed to be deterministic sources [17, 18] that generate a copy of  $|M^\pm\rangle$  each, every  $T_q$  seconds, in each of the  $M$  orthogonal frequency modes. Each source sends one half of  $|M^\pm\rangle$ , i.e., two of the four temporal modes—over each of the  $M$  frequency modes—towards the BSM at the center of the elementary link over a lossy channel. The remaining two modes are loaded to a broadband multi-mode atomic quantum memory [22, 23]. Treating a perfect  $|M^\pm\rangle$  state suffices since all the channel loss (and zero-photon emission probability at the source) can be *pushed* through the beam-splitter of the BSM device into a multiplier to the detection efficiency  $\eta_e$  of the detectors. Upon successful projection by the BSM on one of the two Bell states (the linear-optic BSM never projects on two of the four Bell states)—in at least one of the  $M$  frequencies, which happens with probability  $P_s(1) = 1 - (1 - P_{s0})^M$ , the BSM communicates the which-frequency information to both memories.  $P_{s0}$  is the probability of successful creation of an elementary link for a single frequency mode. We denote the quantum state of a successfully-created elementary link, as  $\rho_1$ .

*Connecting elementary links.*—Each quantum memory receives a pair of which-frequency information from two elementary links (see Fig. 1(b)), which it uses to translate the qubits from the two sides to a pre-determined common frequency [14], and thereafter performs a linear-optic BSM. The BSMs at the repeater nodes do not need to be performed hierarchically (which would require much more classical communication and hence longer-term memories than what our architecture requires). Let us denote the detection efficiencies and dark-click probability per mode for each of the two detectors used for the BSM,  $\eta_r$  and  $P_r$ , respectively. Let  $\lambda_m$  denote a sub-unity transmittance to account for inefficiency in loading (and retrieving) a photon into (and from) the memory. If this BSM is successful, two elementary links are connected to form an entangled state across twice the distance of  $\rho_1$ . We denote the state of this connected segment,  $\rho_2$ . Two

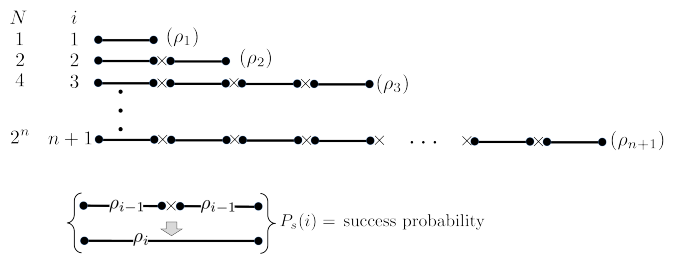


Figure 2. Concatenated linking of  $N = 2^n$  elementary links.

copies of  $\rho_2$  are connected (probabilistically) to produce  $\rho_3$ , and so on. Given two identical copies of  $\rho_{i-1}$ , we denote the probability that one copy of  $\rho_i$  is created,  $P_s(i)$ , for  $1 \leq i \leq n + 1$ .

*Error probabilities and key rate.*—Let us assume that Alice and Bob both make a measurement on each qubit of the entangled state  $\rho_i$  at their respective ends, either in the computational basis (single-photon detection on each of the two modes), or the 45-degree rotated basis (realized by a 50-50 beamsplitter between the two modes of the qubit, followed by single-photon detection on each mode). Let us denote the detection efficiency and dark-click probability per mode for their detectors,  $\eta_d$  and  $P_d$ , respectively. The sift probability  $P_1$  is the probability that Alice and Bob *both* obtain exactly one click in their detectors, provided they both measure in the same basis [?]. Conditioned on this event happening, we denote  $Q_i$  to be the probability the sifted bits Alice and Bob infer are different (despite the fact they deemed the measurement ‘successful’). The error correcting code used to extract shared secure keys must code around this error rate. Clearly, if all detectors in the architecture are noiseless (i.e.,  $P_e = P_r = P_d = 0$ ),  $Q_i = 0$ ,  $1 \leq i \leq n + 1$ . The overall success probability in creating  $\rho_{n+1}$ ,  $P_{\text{succ}} = P_s(n + 1) P_s(n)^2 \dots P_s(2)^{2^{n-1}} P_s(1)^{2^n}$ . If Alice and Bob work with  $\rho_{n+1}$ , i.e., have  $N = 2^n$  elementary links separating them, the unconditionally-secure secret key rate they can extract is given by,

$$R = \frac{P_1 P_{\text{succ}} R_2(Q_{n+1})}{2T_q} \text{ secret-key bits/sec}, \quad (1)$$

where the factor of 2 in the denominator accounts for the probability that Alice and Bob use the same basis choice,  $R_2(Q) = 1 + 2(1 - Q) \log_2(1 - Q) + 2Q \log_2(Q)$  is the secret-key rate of BB84 in bits per sifted symbol, with  $Q$  the error probability in the sifted bit [24]. Refs. [25, 26] generalized (1) for the case when Alice and Bob use a  $d$ -dimensional encoding ( $d > 2$ ), and  $g$  mutually-unbiased measurement bases, with  $2 \leq g \leq d + 1$ .

## II. THEORETICAL ANALYSIS

In this Section, we first summarize our main analytical results, i.e., to derive a fully analytical characterization of the end-to-end shared entangled state (which could

be useful in analyzing other non-QKD applications), and explicit formulas for  $P_{\text{succ}}$ ,  $P_1$ , and  $Q_{n+1}$ , using which the secret key rate can be calculated from Eq. (1). We thereafter provide a sketch of the proofs, with detailed calculations deferred to the Appendices.

**Theorem 1** *Assuming Alice and Bob make a measurement on  $\rho_i$  in the same basis,*

1. Sift probability. *The probability Alice and Bob both obtain exactly one click on their respective detectors (and hence deem their measurement outcomes useful) is given by,  $P_1 = (q_1 + q_2)^2$ , where  $q_1 = (1 - P_d)A_d$  and  $q_2 = (1 - A_d)P_d$ , with  $A_d \equiv \eta_d + (1 - \eta_d)P_d$ , are loss and noise parameters of Alice's and Bob's detectors.*
2. QBER. *Conditioned on a successful sift, the error probability  $Q_i$ , i.e., the probability they obtain mismatched bits, is given by,*

$$Q_i = \frac{1}{2} \left[ 1 - \frac{t_d}{t_r} (t_r t_e)^{2^{i-1}} \right], \quad 1 \leq i \leq n+1, \quad (2)$$

where  $t_e = (1 - 2w_1)/(1 + 2w_1)$ ,  $t_r = (1 - 2w_r)/(1 + 2w_r)$ , and  $t_d = ((q_1 - q_2)/(q_1 + q_2))^2$  are functions of loss-noise parameters of detectors in the elementary links, memory (repeater) nodes, and Alice-Bob, respectively, which become one when the respective detector has zero dark-click probability.  $2w_1 = 2c_e/(a_e + b_e)$ , is the relative probability of classical correlations to that of pure Bell states in the elementary link state  $\rho_1$ .  $2w_r = 2c/(a + b)$  is the fractional probability spillovers to the classical states at each repeater connection. (See Proposition 2 for remaining definitions.)

3. Successful connection probabilities. *The success probability  $P_s(i)$ , to prepare  $\rho_i$  from two copies of  $\rho_{i-1}$ , is given by,  $P_s(1) = s_1 = a_e + b_e + 2c_e$ , and  $P_s(i) = s = a + b + 2c$ , for  $2 \leq i \leq n+1$ . The overall success probability is therefore given by,*

$$P_{\text{succ}} = \frac{1}{4s} [4s(1 - (1 - 4s_1)^M)]^{2^n}. \quad (3)$$

The proof of Theorem 1 involves a detailed analysis of how the quantum states  $\rho_i$  evolve through successive connections of elementary links (sketched in Fig. 2) and finding the exact solution of a variation of the so called *logistic map* (whose solutions are chaotic in general). With the  $Q_i$  as defined above, it is easy to see that,

$$(1 - 2Q_{i+1}) = \frac{t_r}{t_d} (1 - 2Q_i)^2, \quad 1 \leq i \leq n. \quad (4)$$

The pre-factor  $t_r/t_d$  in the above error-propagation law equals one if the detectors at the memory nodes have zero dark clicks ( $P_r = 0 \Rightarrow t_r = 1$ ) and if the detectors used to measure the end points of  $\rho_i$  have zero dark clicks ( $P_d = 0 \Rightarrow t_d = 1$ ). One interesting observation about

the error propagation (4) is that the constant  $t_r$  is only a function of the fractional probability transferred to classical correlations (2c) to that which goes to one of two Bell states ( $a + b$ ), when two pure Bell states are connected by a linear-optic BSM with lossy-noisy detectors (see Proposition 2).

*Proof sketch of Theorem 1.*—We now describe the steps leading up to the proof of the results summarized in Theorem 1. We will defer several details to Appendices A, B, C, D, and E. We first explicitly calculate the quantum state  $\rho_i$  after a given number of elementary links are successfully connected, and thereafter use that to calculate  $Q_i$ ,  $P_1$ ,  $P_{\text{succ}}$ , and eventually the end-to-end secret-key rates using Eq. (1). For our analysis, we can assume without loss of generality that the sources always produce the state  $|M^+\rangle$ . In reality, the sources may produce  $|M^+\rangle$  or  $|M^-\rangle$  probabilistically, but if the signs are known a posteriori (as in an SPDC source), they can be accounted for in post processing at the error-correction stage. In fact, as long as the source produces any one of the four Bell-basis states in each  $T_q$  second, if it is known which one is produced, it can be accounted for with classical post-processing. Let us first consider calculating the states,  $\rho_i$ .

**Proposition 2** *The quantum state  $\rho_i$  obtained after  $i$  connection levels,  $1 \leq i \leq n+1$ , is given by,*

$$\rho_i = \frac{1}{s_i} [a_i|M^+\rangle\langle M^+| + b_i|M^-\rangle\langle M^-| + c_i|\psi_0\rangle\langle\psi_0| + d_i|\psi_1\rangle\langle\psi_1| + d_i|\psi_2\rangle\langle\psi_2| + c_i|\psi_3\rangle\langle\psi_3|], \quad (5)$$

where  $|\psi_0\rangle = |01, 01\rangle$ ,  $|\psi_1\rangle = |01, 10\rangle$ ,  $|\psi_2\rangle = |10, 01\rangle$ ,  $|\psi_3\rangle = |10, 10\rangle$ ,  $|M^\pm\rangle = [|\psi_2\rangle \pm |\psi_1\rangle]/\sqrt{2}$ ,  $s_i = a_i + b_i + 2(c_i + d_i)$  is a normalization constant, and the coefficients of  $\rho_{i+1}$  are recursively given as:

$$a_{i+1} = \frac{1}{s_i^2} [aa_i^2 + (a + b)a_i b_i + bb_i^2], \quad (6)$$

$$b_{i+1} = \frac{1}{s_i^2} [ba_i^2 + (a + b)a_i b_i + ab_i^2], \quad (7)$$

$$c_{i+1} = \frac{1}{s_i^2} [c(a_i + b_i)^2 + 2(a + b)c_i(a_i + b_i + 2d_i) + 4c(d_i(a_i + b_i) + c_i^2 + d_i^2)], \quad (8)$$

$$d_{i+1} = \frac{1}{s_i^2} [4cc_i(a_i + b_i + 2d_i) + 2(a + b)(d_i(a_i + b_i) + c_i^2 + d_i^2)], \quad \text{with} \quad (9)$$

$$s_{i+1} = a_{i+1} + b_{i+1} + 2(c_{i+1} + d_{i+1}), \quad (10)$$

where the parameters,

$$a = \frac{1}{8} [P_r^2(1 - A_r)^2 + A_r^2(1 - P_r)^2], \quad (11)$$

$$b = \frac{1}{8} [2A_r P_r(1 - A_r)(1 - P_r)], \quad (12)$$

$$c = \frac{1}{8} P_r(1 - P_r) [P_r(1 - B_r) + B_r(1 - P_r)], \quad (13)$$

with  $A_r = \eta_r \lambda_m + P_r(1 - \eta_r \lambda_m)$ , and  $B_r = 1 - (1 - P_r)(1 - \eta_r \lambda_m)^2$ , are functions of the system's loss and noise parameters. For  $i = 1$  (the elementary link), we have the initial conditions,  $a_1 = a_e$ ,  $b_1 = b_e$ ,  $c_1 = c_e$ , and  $d_1 = 0$ , with  $s_1 = a_e + b_e + 2c_e$ , where  $a_e, b_e, c_e$  are defined exactly as  $a, b, c$ , with  $(P_e, A_e, B_e)$  replacing  $(P_r, A_r, B_r)$  in Eqs. (6), (7), (8), where  $A_e = \eta_e \lambda + P_e(1 - \eta_e \lambda)$  and  $B_e = 1 - (1 - P_e)(1 - \eta_e \lambda)^2$ , defined similar to  $A_r, B_r$ .

This proposition is proved in Appendix A, where we also calculate the state  $\rho_i$  (i.e., the coefficients  $a_i, b_i, c_i, d_i$ ) explicitly for all  $i$  in terms of the loss and noise parameters. The key steps in the proof are: (i) to realize that the transmittance of half of each elementary link  $\lambda$  and the memory efficiency  $\lambda_m$  at the repeater nodes, can be combined with the detector efficiencies  $\eta_e$  and  $\eta_r$  of the BSMs, respectively, (ii) realizing that a single-photon detector with efficiency  $\eta$  and dark-click probability  $P$ —when the light impinging on it is guaranteed to have no more than 2 photons—is accurately described by the POVM elements,  $F_0 = (1 - P)\Pi_0 + (1 - P)(1 - \eta)\Pi_1 + (1 - P)(1 - \eta)^2\Pi_2$  and  $F_1 = \mathbb{I} - F_0$ , with  $\Pi_i = |i\rangle\langle i|$ ,  $i = 0, 1, 2$  being projectors corresponding to the vacuum, single photon and two photon outcomes of an ideal photon-number-resolving measurement, and, (iii) carrying out the BSM on  $\rho_i^{\otimes 2}$  while accounting for the appropriate post-selections [16].

Once we have the state  $\rho_i$ , defined recursively in terms of  $\rho_{i-1}$ , we calculate the success probabilities,  $P_s(i) = 4s_i$ . The key is to realize that  $s_i = s = a + b + 2c$ ,  $\forall i \geq 2$ , which follows from adding Eqs. (6) and (7). The success probability of creating  $\rho_1$ ,  $P_s(1) = 1 - (1 - P_{s0})^M$ , where  $P_{s0} = 4s_1$  is the probability of successful creation of an elementary link  $\rho_1$  in one of the  $M$  frequencies.

We next prove that the sift-probability  $P_1 = (q_1 + q_2)^2, \forall i$ , where  $q_1 = (1 - P_d)A_d$ ,  $q_2 = (1 - A_d)P_d$ , with  $A_d = \eta_d P_d + 1 - \eta_d$  being parameters of Alice's and Bob's noisy detectors. An intuitive explanation is as follows:  $q_2$  is the probability that the noisy detector 'flips' the outcome ( $|10\rangle$  detected as (no-click, click), or  $|01\rangle$  detected as (click, no-click)), whereas  $q_1$  is the probability that the detector does not flip the outcome ( $|01\rangle$  detected as (no-click, click), or  $|10\rangle$  detected as (click, no-click)). Since the flip and no-flip probabilities are symmetric in the inputs  $|01\rangle$  and  $|10\rangle$ , and each half of  $\rho_i$  has exactly one photon, regardless of the relative fractions of  $|01\rangle$  and  $|10\rangle$  in Alice's and Bob's states, the probability they both get a single-click outcome is  $(q_1 + q_2)^2$ .

The final step is to obtain the error probability  $Q_i = \text{Tr}[\rho_i(M_{0101} + M_{1010})]/\text{Tr}[\rho_i(M_{0101} + M_{0110} + M_{1001} + M_{1010})]$  (note that the denominator is  $P_1$ ), with  $M_{ijkl} \equiv F_i \otimes F_j \otimes F_k \otimes F_l$ . It is simple to argue that  $Q_i$  is a function only of  $2c_i/s_i$  (see Appendix D for detailed proof). The intuitive argument is that a bit error only arises from  $2c_i/s_i$ , the fractional probability of the classical correlation terms in  $\rho_i$ , whereas  $(a_i + b_i)$  is the sum fractional probability of the two Bell states  $|M^+\rangle$  ( $a_i$ ) and  $|M^-\rangle$  ( $b_i$ ), with  $s_i = (a_i + b_i) + 2c_i$ . Even if the BSM results accidentally in a  $|M^-\rangle$  to be formed, there would

be no bit error. In order to calculate  $c_i$ , we calculate  $c_i + d_i \equiv y_i$  and  $c_i - d_i \equiv u_i$  by adding and subtracting Eqs. (8) and (9), and writing recursions for  $y_i$  and  $u_i$ . The solution to  $y_i$  comes out as,  $y_i = (s_i - z_i)/2$ , with  $z_i = (s^2/(a + b))((1 + 2w_1)(1 + 2w_r))^{-2^{i-1}}$ , where  $w_r = c/(a + b)$  and  $w_1 = c_e/(a_e + b_e)$ . The solution to  $u_i$  requires us to solve the following variant of the chaotic logistic map:  $w_{i+1} = w_r + 2(1 - 2w_r)w_i(1 - w_i)$ , where  $w_i = u_i/z_i$ . We derive the exact solution of this quadratic recursion (see Appendix E for proof), and are thus able to evaluate  $Q_i = [1 - t_d(1 - 2c_i/s_i)]/2$ , which simplifies to the form shown in Theorem 1.

Even though our analysis assumed a deterministic entanglement source, it is easy to account for a probabilistic entanglement source with zero multi-pair emissions. Such a probabilistic entanglement source can be modeled as generating  $|\psi\rangle = (1 - p)|0\rangle|0\rangle + p|M^\pm\rangle\langle M^\pm|$  every  $T_q$  seconds. Since  $|\psi\rangle$  can be regarded as the quantum state obtained by passing  $|M^\pm\rangle$  through a beamsplitter of transmittance  $p$ , we can 'push'  $p$  through the BSM at the centers of elementary links, and apply our formulas after replacing  $\lambda\eta_e$  by  $\lambda\eta_e p$ , and accordingly modifying the elementary link parameters:  $a_e, b_e, c_e$ .

Finally, even though all the above analysis was done for  $N = 2^n$  elementary links (with  $n$  an integer), we believe that the final formula for  $Q$  and rate also hold for any integer  $N$ . In other words, with an end-to-end optical fiber channel with  $N$  elementary links,

$$R = \frac{P_1 P_{\text{succ}} R_2(Q(N))}{2T_q} \text{ secret-key bits/sec}, \quad (14)$$

where,  $Q(N) = \frac{1}{2} \left[ 1 - (t_d/t_r) (t_r t_e)^N \right]$ . Since  $R(Q) = 1 - 2h_2(Q)$ , with  $h_2(x) = -x \log_2(x) - (1 - x) \log_2(1 - x)$  the binary entropy function, the maximum range for which QKD is possible at a non-zero rate is determined by when  $Q(N)$  falls below  $Q_{\text{th}}$ , where  $h_2(Q_{\text{th}}) = 1/2$ .  $Q_{\text{th}} \approx 0.1104$ . One can invert  $Q(N)$  to derive the maximum range as a function of number of elementary links  $N$ , and all the detector loss and noise parameters:

$$L_{\text{max}} = \frac{20N}{\alpha} \log_{10} \left[ \frac{\eta_e}{8P_e} \left( \sqrt{8(1 - 2P_e)H} - 4(1 - 2P_e) \right) \right],$$

where  $H = 1 + t_r / \left[ (1 - 2Q_{\text{th}}) \frac{t_r}{t_d} \right]^{\frac{1}{N}}$  and  $\alpha$  is the fiber loss coefficient, in dB/km.

### III. NUMERICAL ANALYSIS

*Main results.*—Our main numerical results, described in detail in this section, are summarized below.

- 1. Simulation of lossy linear optics and noisy detectors.** We set up a full numerical simulation, using the sparse matrix toolbox of MATLAB to create time-efficient subroutines for beam-

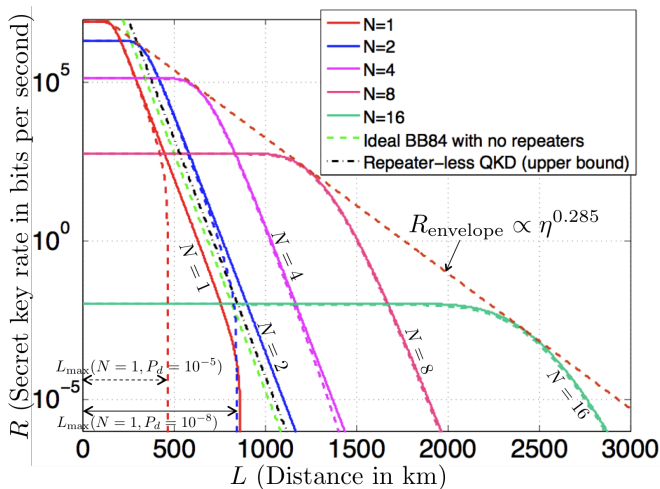


Figure 3. Secret key rate  $R$  as a function of range  $L$  assuming ideal entanglement sources ( $p(2) = 0$ ). The rate-distance envelope attained (over 1, 2, 4, 8 and 16 elementary links)—for the chosen lossy-noisy device parameters—is seen to outperform what is theoretically achievable by any repeater-less QKD implementation that uses the same time-slot length ( $T_q$ ) and number of frequency channels ( $M$ ), for total range  $L \geq 260$  km. The figure also shows a power-law fit to the envelope,  $R \propto \eta^{0.285}$ , which outperforms the  $R \propto \eta$  scaling of repeater-less QKD. The parameter values we chose are:  $P_d = P_r = P_e = 10^{-8}$  (solid lines),  $P_d = P_r = P_e = 10^{-5}$  (dashed lines),  $\eta_d = \eta_r = \eta_e = 0.9$ ,  $\lambda_m = 1$  dB (memory loss),  $M = 1000$  (frequency modes),  $\alpha = 0.15$  dB/km (fiber loss), and  $T_q = 50$  ns (time-slot length).

splitters, partial trace operations, and photon-number-resolving detectors, for efficiently simulating continuous-variable quantum dynamics on bosonic systems. We use this tool to simulate the repeater chain architecture described above, where all photon detectors in the system are assumed to have only single-photon resolution. This numerical tool may find use in several future applications.

- 2. Rate-vs.-loss scaling.** We use our tool to simulate the repeater-chain architecture, and evaluate secret-key rates as a function of distance. For an entanglement source with no 2 or higher photon-pair terms, the results from the theory and numerics are seen to match exactly. We show that our repeater architecture outperforms the  $R \sim \eta$  scaling of secret key rate  $R$  as a function of channel transmittance  $\eta$ , which any QKD protocol with no repeaters must be limited to [7]. The envelope of the rate-loss tradeoff over the different number of elementary links was found to scale as  $R = \eta^s$  for some parameter  $s \in (0, 1)$  that depends on the system parameters (see Fig. 3).
- 3. Sources with non-zero two-pair emission probability.** We numerically evaluate the performance of the repeater architecture when the

sources have non-zero two-pair emission rates ( $p(2) > 0$ ). We find that for any given value of  $p(2)$ , up to a certain maximum number of elementary links  $N_{\text{max}}(p(2))$ , the rate-distance performance remains almost the same as attained by an ideal ( $p(2) = 0$ ) source, but the rate drops quickly to zero if  $N > N_{\text{max}}(p(2))$  elementary links are used (see Fig. 4).

- 4. Error propagation.** Our numerical simulations show that the scaling law in Eq. (4) we derived for error-propagation through the repeater chain holds—with an appropriate  $p(2)$ -dependent modification to the pre-factor ( $t_r/t_d$ )—even for non-ideal sources (see Fig. 6).

*Detailed description of numerical results.*—In Fig. 3, we plot the secret key rate as a function of range with  $N = 2^n$  elementary links, with  $n = 0, 1, 2, 3, 4$ , for all system parameters held the same (see figure caption for the actual values used), but two different values of the dark-click probability of all the detectors in the system,  $P_d = 10^{-5}$ , and  $P_d = 10^{-8}$ . The first three plots ( $N = 1, 2, 4$  elementary links) were computed both using the theoretical formula as well as the numerical simulation, and they match exactly. Following are key observations:

1. The envelope of the key rate (over all  $N$ ) is close to identical for the two values of dark click probability. The maximum range  $L_{\text{max}}$  achievable by a given total number of elementary links, however, drastically decreases with increasing  $P_d$ .
2. At a given  $L$ , the range should be divided into an optimum number ( $N$ ) of elementary links, to maximize the rate. At short distances, using too many repeaters diminishes the end-to-end key rate, due to the 50% heralding efficiencies of the linear-optic BSMs at the repeater nodes connecting pairs of elementary links.
3. The secret key rate of any QKD protocol that does not use quantum repeaters must be upper bounded by  $R \leq \log((1 + \eta)/(1 - \eta))$  bits per mode [7],  $\eta$  being the total channel transmittance, which roughly equals  $R \approx 2.88\eta$ , when  $\eta \ll 1$  (high loss). The BB84 protocol—both the single-photon based and the weak coherent state implementation employing decoy states—as well as the continuous-variable (CV) QKD protocol attain a key rate performance given by  $R \approx \eta$  [27], thereby leaving little room for improvement by any other protocol. We show that our repeater architecture attains a rate-loss tradeoff that outperforms this fundamental rate-loss scaling that any protocol not using repeaters must adhere to (when given the same time-slot width  $T_q$ , and the same number of orthogonal frequency modes  $M$ , for a fair comparison). The envelope of the rate-loss tradeoff over the different number of elementary links is found to scale

as a power law, i.e.,  $R = \eta^s$  for some parameter  $s \in (0, 1)$  that depends on the system parameters, as depicted in Fig. 3.

In Fig. 4, we plot the secret key rates for  $N = 1, 2, 4, 8$  elementary links ( $n = 0, 1, 2, 3$ ) with all parameters held constant,  $p(1) = 0.9$  and several choices of  $p(2)$  ranging from 0.001 to 0.015. We model the non-ideal entanglement source as generating the state [31],

$$|\psi\rangle = \sqrt{1-p(1)-p(2)}|00,00\rangle + \sqrt{p(1)}|M^+\rangle + \sqrt{p(2)/3}(|20,02\rangle + |11,11\rangle + |02,20\rangle), \quad (15)$$

where  $|M^+\rangle = [|10,01\rangle + |01,10\rangle]/\sqrt{2}$ . This form of the state, and in particular of the 4-photon term, is motivated by parametric down-conversion sources [32]. If  $p(2)$  is small, the exact form of the two-pair term does not seem to affect the results, notwithstanding that our simulation is easily able to take into account any particular form of the two-pair term, depending upon the physical model of the actual source of entanglement. Finally, we assume that the higher-order multi-pair emission terms (3-pair or higher) have significantly lower probabilities compared to the two-pair term, and that  $p(2)$  effectively captures the effect of multi-pair emissions to the secret-key rates. The key observations from Fig. 4 are as follows [33]:

1. For non-ideal sources (i.e.,  $p(2) > 0$ ), At any given value of  $p(2)$ , there is a maximum number  $N_{\max}$  of elementary links up until which the rate-loss envelope achieved by the repeater architecture remains almost identical to what is achieved by a  $p(2) = 0$  entanglement source. However, as soon as  $N$  exceeds  $N_{\max}(p(2))$ , the rate crashes to zero.
2. Interestingly, the rate-distance plots in Fig. 4 are seen to come crashing down from higher  $N$  values to lower  $N$  values (number of elementary links) *one at a time* as  $p(2)$  is increased upwards from 0 (with  $p(1) = 0.9$  held constant), while the rate-distance tradeoffs for a lower  $N$  value stays unaffected, i.e., almost at its  $p(2) = 0$  level, until  $p(2)$  becomes high enough to make that value of  $N$  unsustainable. As an example, note that the  $N = 1$  plot has no perceivable change from  $p(2) = 0.001$  to  $p(2) = 0.055$ . Similarly, the  $N = 2$  plot has no perceivable change from  $p(2) = 0.001$  to  $p(2) = 0.019$ .

In Fig. 5, we plot the end-to-end QBER when a fixed overall range  $L$  (of 10 km, and 590 km) is divided up into 1, 2, 4 or 8 elementary links. The color convention of the plots in Fig. 5 is the same as the one used for the secret key rate plots in Fig. 4. The black horizontal lines correspond to  $Q_{\text{th}} = 0.1104$ . The secret key rate goes to zero when the end to end QBER falls below  $Q_{\text{th}}$ . It is instructive to tally the  $p(2)$  values where  $Q_{n+1}$  crosses the  $Q_{\text{th}}$  line for  $n = 0, 1, 2, 3$ , with the plots in Fig. 4. The  $p(2)$  value when the 8-elementary-link chain's maximum

range is 590 km, is 0.0054, and that when it is 10 km is 0.0084, both of which match well with the plots (c) and (d) of Fig. 4. Similarly, the  $p(2)$  value when the 4-elementary-link chain's maximum range is 590 km, is 0.0116, and that when it is 10 km is 0.0195, which match well with plot (g) of Fig. 4. Finally, the  $p(2)$  value when the 2-elementary-link chain's maximum range is 590 km, is 0.0347, and that when it is 10 km is 0.0577, which match well with plots (j), (k) and (l) of Fig. 4.

In Fig. 6(a), we depict our  $L$ -km-range,  $N = 2^n$  elementary-link construction, for  $n = 3$ . The Alice-to-Bob range  $L$  is divided up into  $N = 2^n$  elementary links, and  $Q_i$  is defined as the error probability if Alice and Bob were to measure the state  $\rho_i$  (which is formed after successfully connecting  $2^{i-1}$  elementary links, each of length  $L/N$ ),  $1 \leq i \leq n+1$ . In Fig. 6(b), we plot  $Q_i$  as a function of  $p(2)$ , when  $p(1) = 0.9$  is held fixed, with  $p(0) = 1 - p(1) - p(2)$ , for  $N = 2^n$ , with  $n = 3$ . At each value of  $i \in \{0, 1, 2, 3\}$ , the respective QBER  $Q_{i+1}$  seems to grow almost linearly with  $p(2)$  when  $p(2)$  is small, for chosen system parameters as mentioned in the caption of Fig. 6. In Fig. 6(c), we plot the ratio,  $C(p(2)) = (1 - 2Q_{i+1})/(1 - 2Q_i)^2$  for  $i = 1, 2, 3$ , as a function of  $p(2)$ . For the ideal source ( $p(2) = 0$ ), we proved above that the QBER ratio  $C(p(2)) = t_r/t_d$ , which is independent of  $i$  (4). For the aforesaid loss and noise parameters,  $t_r/t_d = 1 - \epsilon$ , with  $\epsilon = 1.39 \times 10^{-5}$ . We see here numerically, that  $C(p(2))$  is independent of  $i$ , *even for an imperfect source*, for any value of  $p(2) \in [0, 0.055]$ . The ratio has a good fit to the line,  $C \approx (t_r/t_d) - 4p(2)$  for the above range of  $p(2)$ . The  $p(2)$ -dependence of  $C$  deviates from linear as  $p(2)$  becomes higher. This is quite interesting, as this gives us a way to predict the end-to-end QBER on long repeater chains by making a physical measurement on one noisy elementary link, if similar devices are used to construct each elementary link.

Finally, leveraging our empirical verification of the QBER scaling law for  $p(2) > 0$ , we will derive an estimate the form of the  $p(2)$  dependence of  $N_{\max}$ , the maximum usable number of elementary links of a given range and quality. In Fig. 7(a), we plot  $1 - 2Q_1$ , with  $Q_1$  the QBER of one elementary link (of range  $L_{\text{elem}} = L/N$ , chosen in the range 50 km to 550 km), as a function of  $p(2)$ . It is seen that,  $1 - 2Q_1 \gtrsim t_d t_e - \frac{1}{2}p(2)$ . This linear approximation seems good for elementary links of range below 400 km, and for  $p(2) < 0.02$ . Putting this together with the linear approximation of the constant in the QBER scaling law, i.e.,  $1 - 2Q_{i+1} \gtrsim (t_r/t_d - 4p(2))(1 - 2Q_i)^2$ ,  $i \geq 1$ , we get,

$$\log(1 - 2Q_i) \gtrsim \left(\frac{t_r}{t_d} - 4p(2)\right)^{2^{i-1}} \left(t_d t_e - \frac{1}{2}p(2)\right)^{2^{i-1}}, \quad (16)$$

which upon simplification yields,

$$2^i \gtrsim \frac{|\log(1 - 2Q_i) + \log(t_r/t_d - 4p(2))|}{\left|\frac{1}{2}\log(t_d t_e - \frac{1}{2}p(2)) + \log(t_r/t_d - 4p(2))\right|}. \quad (17)$$

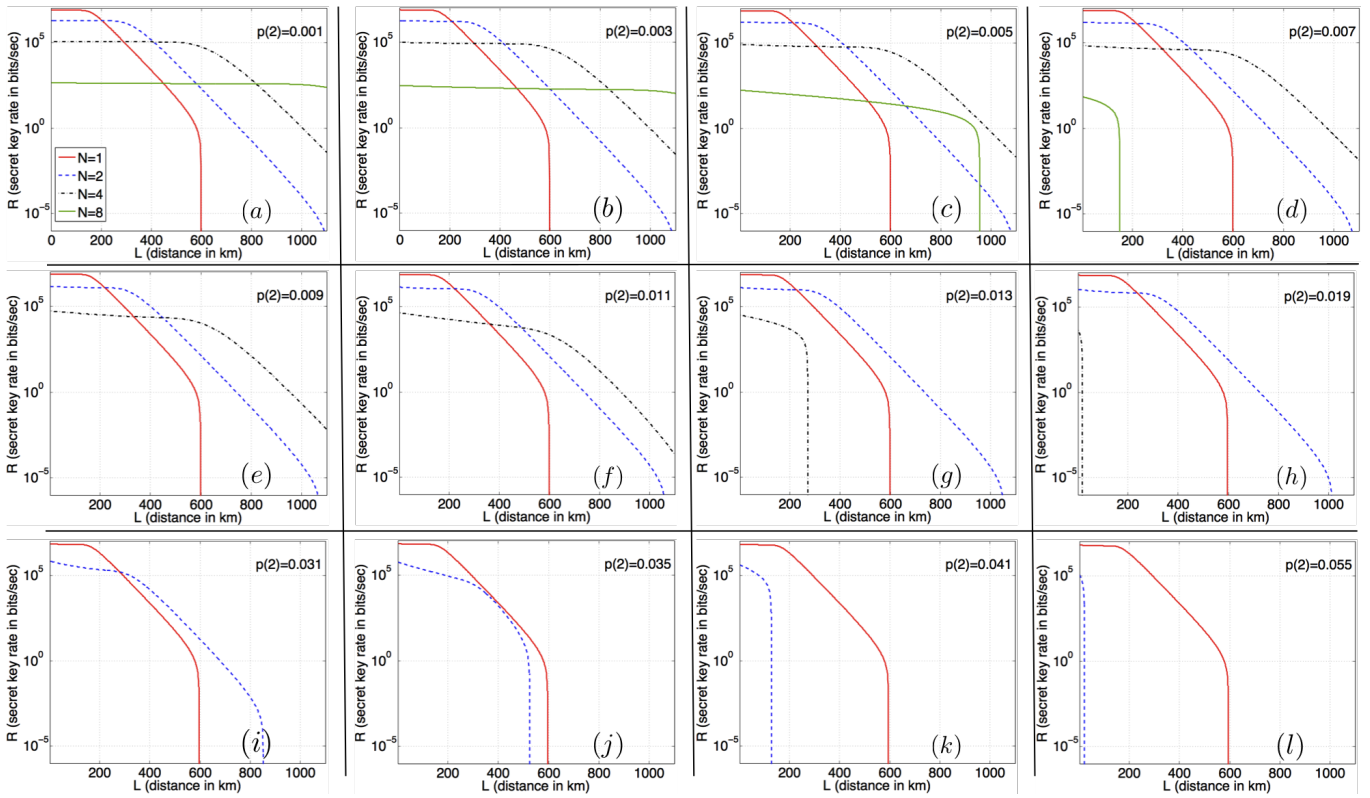


Figure 4. Secret key rate vs. distance, evaluated for  $n = 0, 1, 2, 3$  ( $N = 1, 2, 4, 8$  elementary links), for sources with two-pair emission probability  $p(2)$  ranging from 0.001 to 0.055. At any given value of  $p(2)$ , there is a maximum number  $N_{\max}$  of elementary links up until which the rate-loss envelope achieved by the repeater architecture remains almost identical to what is achieved by a  $p(2) = 0$  entanglement source. However, as soon as  $N$  exceeds  $N_{\max}(p(2))$ , the rate goes to zero. The parameter values used are:  $P_d = P_r = P_e = 10^{-6}$ ,  $\eta_d = \eta_r = \eta_e = 0.9$ ,  $\lambda_m = 1$  dB (memory loss),  $M = 1000$  (frequency modes),  $\alpha = 0.15$  dB/km (fiber loss), and  $T_q = 50$  ns. The plots show that, for these parameters, for  $p(2) = 0.035$ , it is best to have a single elementary link between Alice and Bob over the entire range. The rate-loss tradeoff for 2 elementary links is worse at all range values. Similarly, at  $p(2) = 0.013$ , using 4 elementary links does not yield a better rate compared to what is attained with 2 elementary links, at all range values. Interestingly however, the rate-distance plots come crashing down from higher  $N$  values to lower (number of elementary links) *one at a time* as  $p(2)$  is increased, while the rate-distance tradeoffs for the lower  $N$  values stay almost at their  $p(2) = 0$  levels. Note that the  $N = 1$  plot has no perceivable change from  $p(2) = 0.001$  to  $p(2) = 0.055$ . Similarly, the  $N = 2$  plot has no perceivable change from  $p(2) = 0.001$  to  $p(2) = 0.019$ .

The secret key rate  $R$  goes to zero when  $1 - 2Q_i < 1 - 2Q_{\text{th}} \approx 0.78$ . Substituting  $\log(1 - 2Q_{\text{th}}) \approx -0.25$ ,  $\log(1 - x) \approx -x - x^2/2$ , and  $t_r = t_d = t_e = 1$  (in order to capture the  $N_{\max}(p(2))$  dependence, and do so in the low-noise regime of the elementary links), and ignoring the  $\mathcal{O}(p(2)^2)$  terms, we obtain the following approximation,

$$N_{\max} \gtrsim (16/17) + \frac{1/17}{p(2)}, \quad (18)$$

which is roughly a shifted hyperbolic dependence in  $p(2)$ . The above interpretation of  $N_{\max}$  is that it is the maximum number of length  $L_{\text{elem}}$  elementary links that can be connected before the concatenation becomes useless for QKD. The ‘quality’ of the elementary link is captured by the parameter  $t_e$ , which is 1 when the dark click probability of the detectors at the center of the elementary link,  $P_e = 0$ . In Fig. 7(b), we plot  $t_e$  as a function of the length of the elementary link  $L_{\text{elem}} \equiv L/N$ ,

for  $P_e = 10^{-6}$ ,  $\eta_e = 0.9$ , and  $\alpha = 0.15$  dB/km. For  $L_{\text{elem}} < 400$  km,  $t_e$  is seen to remain close to 1. This justifies substituting  $t_e = 1$  in order to arrive at Eq. (18). The table in Fig. 5(c) shows that the  $N_{\max}(p(2))$  lower estimate we obtained indeed matches very well with the exact values obtained numerically shown in Figs. 5(a–b).

#### IV. CONCLUSIONS

Long-distance entanglement distribution at high rates is of paramount importance to many quantum communication protocols, the realization of which requires building a network of quantum repeaters. Several quantum repeater protocols have been proposed [9–12, 14], all of which use some source of entanglement, some form of quantum memories, and linear-optics-based Bell-state measurements. We analyzed the architecture

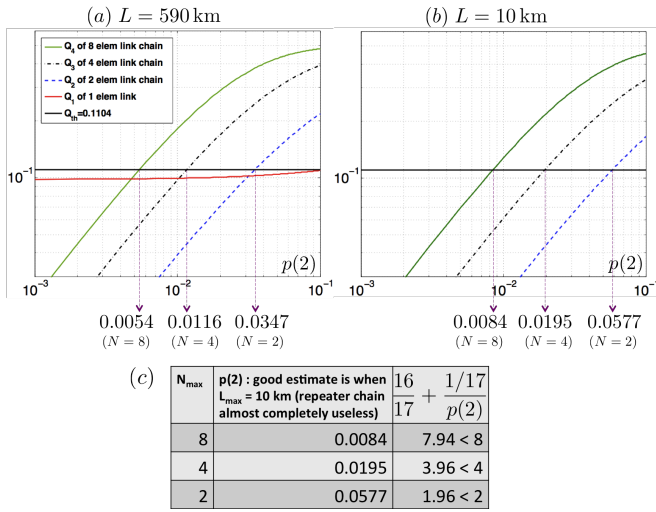


Figure 5. The purpose of this figure is to gauge the  $p(2)$  values where a certain length  $N$  (and higher) of the repeater chain becomes ineffective, as depicted in Fig. 4. We choose two fixed *maximum* range values: one a number close to zero (10 km) to assess  $N_{\max}(p(2))$ , and the other a little below the range of a single elementary link (590 km). We divide an overall range  $L$  of (a) 10 km and (b) 590 km, into  $N = 1, 2, 4$  and 8 elementary links, and plot the end-to-end QBER for each case, as a function of the two-pair-emission probability  $p(2)$ . The black horizontal line corresponds to  $Q_{\text{th}} = 0.1104$ . The secret key rate goes to zero, when the end to end QBER falls below  $Q_{\text{th}}$ . It is instructive to tally the  $p(2)$  values where  $Q_{n+1}$  crosses the  $Q_{\text{th}}$  line for  $n = 0, 1, 2, 3$ , with the plots in Fig. 4. We assume,  $\eta_e = \eta_r = \eta_d = 0.9$ ,  $P_e = P_r = P_d = 10^{-6}$ ,  $\alpha = 0.15\text{dB/km}$ , and  $\lambda_m = 1\text{dB}$ .

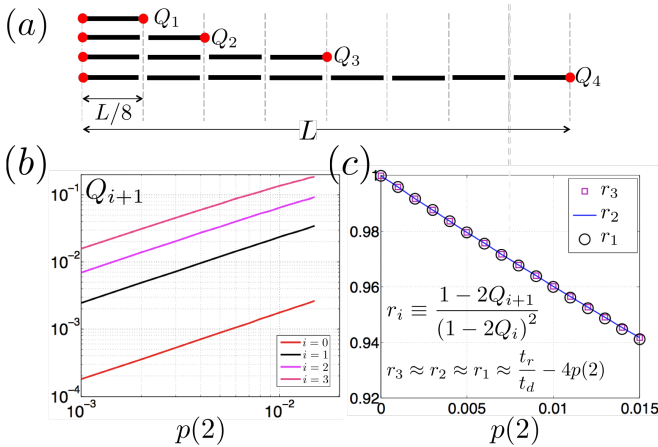


Figure 6. QBER,  $Q_{n+1}$  vs. two-pair-emission probability  $p(2)$ , for different numbers of swaps ( $n = 0, 1, 2, 3$ ) at a fixed distance of  $L = 50$  km (a short range is chosen to ensure that for all four cases the elementary-link quality is very good for the entire  $p(2)$  range we consider, so that we cleanly capture the effect of  $p(2)$  on the QBER). We assume,  $\eta_e = \eta_r = \eta_d = 0.9$ ,  $P_e = P_r = P_d = 10^{-6}$ ,  $M = 1000$ ,  $\alpha = 0.15\text{dB/km}$ ,  $\lambda_m = 1\text{dB}$ , and  $T_q = 50\text{ns}$ .

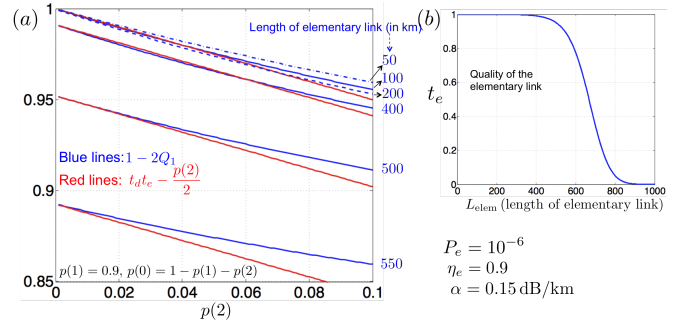


Figure 7. (a) Plot of  $1 - 2Q_1$ , where  $Q_1$  is the QBER of one elementary link (of range  $L_{\text{elem}} = L/N$ , chosen in the range 50 km to 550 km), as a function of  $p(2)$ . It is seen that,  $1 - 2Q_1 \gtrsim t_d t_e - \frac{1}{2}p(2)$ . (b) Plot of  $t_e$ , the ‘quality’ of one elementary link, as a function of  $L_{\text{elem}}$ , for  $P_e = 10^{-6}$ ,  $\eta_e = 0.9$ , and  $\alpha = 0.15\text{dB/km}$ . For  $L_{\text{elem}} < 400$  km,  $t_e$  is seen to remain close to 1.

proposed in [14], which is a repeater protocol that has a superior classical communication overhead, and does not rely on purification of noisy shared entangled pairs. Our analysis should easily carry over to other repeater architectures.

We solved exactly for the quantum state after a given number of swap stages in a concatenated quantum-repeater chain that uses heralded linear-optic Bell-state measurements (BSM). We exploit the fact that if we start with an ideal single-pair entanglement source, the post-selected state after a successful BSM remains in a subspace spanned by only single photon terms, and we recursively evaluate the end-to-end entangled state using an exact model for the noisy single-photon detectors. This calculation required us to exactly solve a variant of the *logistic map* from chaos theory. Using our expression for the quantum state, we determined quantities such as the success probability of entanglement swapping at any given swap level, the error rate of the raw bits obtained by Alice and Bob in a QKD application if they were to measure this state in the same bases, and the sifting probability. One can find any other quantity of interest from the state, such as the entanglement of formation or the fidelity with the maximally entangled state (see Appendix D for the exact expression of fidelity of the  $N$ -elementary link end-to-end state). Our analysis takes into account all major imperfections of the detectors (such as detection efficiencies, and dark click probabilities) and the channel (such as transmissivity and thermal noise, where the latter can be included into an effective dark-click probability term). We also evaluate an exact scaling law for how the quantum bit error rate (QBER) evolves from one swap level to the next, which we found to hold also when the entanglement source is imperfect, i.e., when the two-pair-emission probability is non-zero. This is of great practical importance since it gives us a way to calculate the QBER on long repeater chains by making a physical measurement on one noisy elementary link. Finally, we simu-

lated the repeater-chain architecture, and the QKD protocol numerically, using an efficient model we developed for simulating bosonic states, linear-optic unitaries, and noisy measurements. We found that when the two-pair probability  $p(2)$  is non-zero, the rate-distance tradeoff plots—with  $N$  elementary links dividing up the entire range  $L$  km—are almost unaffected (i.e., remain almost at their  $p(2) = 0$  levels at any  $L$ ), for all  $N$  up to a maximum value  $N_{\max}$ , where  $N_{\max}(p(2))$  decreases as  $p(2)$  is increased. If more than  $N_{\max}(p(2))$  elementary links are used, the key rate is worse at all  $L$  compared to when fewer elementary links are used.

One can in principle replace the linear-optic entanglement swapping scheme with more advanced schemes with improved heralding efficiencies, such as the one proposed by Grice [28] that injects entangled states into a beamsplitter network and heralds total number of clicks from an array of photon-number-resolving detectors, one that uses inline squeezers to beat the 50%-efficiency limit of a linear-optic BSM [29], and another recent proposal that can attain 75% heralding efficiency via linear-optics and injection of (un-entangled) single-photons [30]. Our theoretical technique can be readily used to analyze the repeater-chain architecture when the BSMs are replaced by one of the aforesaid schemes. At each swap stage, after the post-selection by the BSM, the projected shared state will still lie in the span of the 4-mode 2-qubit ‘dual-rail’ basis, but there will be two extra coefficients to track, since the advanced BSMs can identify all four Bell states (as opposed to only two by the linear-optic scheme [16]). It is quite likely that the final expression for  $Q_i$ , and the error-propagation law will still depend upon  $t_d$ ,  $t_r$ , and

$t_e$ , where the latter two are the same functions of the fractional probability transfer to classical correlations at each swap stage (which should be smaller compared to when the linear-optic BSM is used). Finally, our numerical model allows us to simulate these enhanced schemes as well, and also introduce other non-idealities such as finite memory times at the repeaters, non-linearities in the fiber and memories, and temporal detector non-idealities such as timing jitter and after-pulsing rates. The analysis of the repeater chain with the advanced BSM schemes is left for future work.

## ACKNOWLEDGMENTS

The authors would like to thank Khabat Heshami, Gregory Kanter and Yuping Huang for useful discussions. SG thanks Rodney Van Meter and Mohsen Razavi for detailed feedback on an earlier version of this manuscript. This paper is based on research funded by the DARPA Quiness program subaward contract number SP0020412-PROJ0005188, under prime contract number W31P4Q-13-1-0004. WT, a senior fellow of the Canadian Institute for Advanced Research (CIFAR), also acknowledges support from Alberta Innovates Technology Futures (AITF). The views and conclusions contained in this document are those of the authors and should not be interpreted as representing the official policies, either expressly or implied, of the Defense Advanced Research Projects Agency or the U.S. Government.

- 
- [1] A. Ekert, Phys. Rev. Lett. **67**, 6 (1991).
  - [2] C. H. Bennett, G. Brassard, C. Crépeau, R. Jozsa, A. Peres, and W. K. Wootters, Phys. Rev. Lett. **70**, 1895–1899 (1993).
  - [3] C. Bennett and S.J. Wiesner, Phys. Rev. Lett. **69**, 2881 (1992).
  - [4] M. M. Wilde and M.-H. Hsieh, Quantum Information Processing **11**, 6, 1431–1463 (2012).
  - [5] M. M. Wilde, P. Hayden, and S. Guha, Phys. Rev. Lett. **108**, 140501 (2012).
  - [6] S. Guha, J. H. Shapiro, and B. I. Erkmen, “Capacity of the Bosonic Wiretap Channel and the Entropy Photon-Number Inequality”, Proc. of the IEEE International Symposium on Information Theory (ISIT), (2008).
  - [7] M. Takeoka, S. Guha, and M. M. Wilde, to appear in *Nature Communications* (2014).
  - [8] R. Namiki, O. Gittsovich, S. Guha, and Norbert Lütkenhaus, arXiv:1410.0716 [quant-ph] (2014).
  - [9] N. Sangouard, C. Simon, H. de Riedmatten, and N. Gisin, Rev. Mod. Phys. **83**, 33 (2011).
  - [10] H.-J. Briegel, W. Dür, J. I. Cirac, and P. Zoller, Phys. Rev. Lett. **81**, 5932 (1998).
  - [11] L.-M. Duan, M. D. Lukin, J. I. Cirac, and P. Zoller, Nature **414**, 413–418, 22 November (2001).
  - [12] L. Jiang, J. M. Taylor, K. Nemoto, W. J. Munro, R. Van Meter, and M. D. Lukin, Phys. Rev. A **79**, 032325 (2009).
  - [13] S. Bratzik, H. Kampermann, and D. Bruß, Phys. Rev. A **89**, 032335 (2014).
  - [14] N. Sinclair, E. Saglamyurek, H. Mallahzadeh, J. A. Slater, M. George, R. Ricken, M. P. Hedges, D. Oblak, C. Simon, W. Sohler, and W. Tittel, Phys. Rev. Lett., **113**, 053603 (2014).
  - [15] S. L. Braunstein, and A. Mann, Phys. Rev. A *Rapid Communications* **51**, 3 (1995).
  - [16] N. Lütkenhaus, J. Calsamiglia, and K.-A. Suominen, Phys. Rev. A **59**, 3295 (1999).
  - [17] A. Dousse *et al.*, Nature **466**, 217 (2010).
  - [18] Y. Huang and P. Kumar, Phys. Rev. Lett. **108**, 030502 (2012).
  - [19] A. Khalique, W. Tittel, and B. C. Sanders, Phys. Rev. A **88**, 022336 (2013).
  - [20] M. Razavi, H. Farmanbar, and N. Lütkenhaus, Optical Fiber Communication (OFC) Conference, San Diego, California, United States, February 24–28 (2008).
  - [21] E. Schröder, “Über iterierte Funktionen”, Math. Ann. **3** (2): 296–322, doi:10.1007/BF01443992 (1870).
  - [22] E. Saglamyurek, N. Sinclair, J. Jin, J. A. Slater, D. Oblak, F. Bussi eres, M. George, R. Ricken, W. Sohler, and

- W. Tittel, Nature **469**, 512 (2011).
- [23] M. Afzelius, C. Simon, H. de Riedmatten, and N. Gisin, Phys. Rev. A **79**, 052329 (2009).
- [24] P. Shor and J. Preskill, Phys. Rev. Lett **85**, 441–444, (2000).
- [25] A. Ferenczi and N. Lütkenhaus, Phys. Rev. A **85**, 052310 (2012).
- [26] Z.-X. Xiong, H.-D. Shi, Y.-N. Wang, L. Jing, J. Lei, L.-Z. Mu, and H. Fan, Phys. Rev. A **85**, 012334 (2012).
- [27] Scarani *et al.*, Rev. Mod. Phys., **81**, No. 3, July-September (2009).
- [28] W. P. Grice, Phys. Rev. A **84**, 042331 (2011).
- [29] H. A. Zaidi and P. van Loock, Phys. Rev. Lett. **110**, 260501 (2013).
- [30] F. Ewert and P. van Loock, Phys. Rev. Lett. **113**, 140403 (2014).
- [31] C. Śliwa and K. Banaszek, Phys. Rev. A **67**, 030101(R) (2003).
- [32] G. A. Durkin, C. Simon, and D. Bouwmeester, Phys. Rev. Lett. **88**, 187902 (2002).
- [33] H. Krovi, Z. Dutton, S. Guha, C. A. Fuchs, W. Tittel, C. Simon, J. A. Slater, K. Heshami, M. P. Hedges, G. S. Kanter, Y.-P. Huang, and C. Thiel, *to be published*, Proceedings of the Conference on Lasers and Electro-Optics (CLEO), June 8-13, San Jose, CA, (2014).
- [34] H. Krovi, S. Guha, Z. Dutton, C. A. Fuchs, J. Slater, C. Simon, and W. Tittel, *in preparation*, (2014).

## Appendix A: Proof of Proposition 2: Quantum state of the elementary link, and entangled state propagation through a sequence of swap stages

### 1. Elementary link

We first prove Proposition 2 for the case  $i = 1$ , and derive the post-selected quantum state of the elementary link. Let us first consider how we should model non-ideal photodetectors. Ideally we would like to say that each of the four detectors required for the BSM individually measures a Hermitian operator with eigen-projectors  $\{\Pi_0, \Pi_1, \Pi_2\}$ , the  $\Pi_n = |n\rangle\langle n|$  signifying the presence of  $n$  photons. Next we note that we are allowed to limit ourselves to a three-dimensional subspace of the Fock space because we know we will never have more than two photons at a detection site (since we limit the theoretical part of analysis to the case when the sources have  $p(2) = 0$  and assume that any thermal noise in the channel is negligible at typical optical frequencies). The detectors are assumed to have a sub-unity detection efficiency  $\eta_e$ —which may be thought of as arising from a beamsplitter with transmissivity  $\eta_e$  just in front of an ideal detector—and independently there may also be a probability  $P_e$  for the detector to trigger in the absence of a photon. This means the “no click” and “click” events in the individual detectors really correspond to a two-outcome POVM  $\{F_0, F_1\}$ , with

$$F_0 = (1 - P_e)\Pi_0 + (1 - A_e)\Pi_1 + (1 - B_e)\Pi_2 \quad (\text{A1})$$

$$F_1 = P_e\Pi_0 + A_e\Pi_1 + B_e\Pi_2. \quad (\text{A2})$$

where we take

$$A_e = 1 - (1 - P_e)(1 - \eta) \quad (\text{A3})$$

$$B_e = 1 - (1 - P_e)(1 - \eta)^2. \quad (\text{A4})$$

The way to understand  $F_0$ , the “no click” signal for instance, is this: If there are no actual photons present, one will get this outcome with probability  $1 - P_e$ , the probability for no false alarm at the detector. On the other hand, if there is a single photon present both it must disappear and there still be no false alarm; hence a coefficient  $(1 - P_e)(1 - \eta)$  in front of  $\Pi_1$ . Finally, for the case that two photons are present, both of them must be lost and yet no false alarm must appear; hence a coefficient of  $(1 - P_e)(1 - \eta)^2$ .

We next note that we may incorporate the channel transmittance  $\lambda$  (corresponding to propagation loss of each of the halves of the Bell pairs from two ends of the elementary link) directly into the detection efficiency  $\eta_e$ , by defining an effective detection efficiency  $\eta_e\lambda$  while assuming the channel is lossless, rather than accounting for the channel loss in our description of the quantum states arriving at them. One can see this through a simple bosonic mode-operator analysis including two stages of loss, but the intuition should be clear. Consequently, at the center of an elementary link we can assume the state it will attempt to link is a clean  $|M^+\rangle|M^+\rangle$ , while the four detectors in the BSM are working at efficiency

$$\eta = \eta_e\lambda. \quad (\text{A5})$$

This greatly simplifies the analysis by not having to treat the states to be linked as mixed states.

For the purposes of this proof, let us label the four spatial modes involved in an elementary link by  $a, b, c$ , and  $d$ , so that the initial quantum state is more explicitly  $|M_{ab}^+\rangle|M_{cd}^+\rangle$ . The BSM will be applied to modes  $b$  and  $c$ . What this entails is that the modes first impinge on a 50-50 beamsplitter, which enacts a mode transformation

$$b_j^\dagger \longrightarrow \sqrt{\frac{1}{2}}(b_j^\dagger + c_j^\dagger) \quad \text{and} \quad c_j^\dagger \longrightarrow \sqrt{\frac{1}{2}}(b_j^\dagger - c_j^\dagger). \quad (\text{A6})$$

The consequence of this is that the state presented to the photo detectors is a massively entangled one:

$$\begin{aligned} |\text{swap}\rangle = & \frac{1}{4} [ |10, 11, 00, 01\rangle - |10, 01, 10, 01\rangle \\ & + \sqrt{2}|10, 02, 00, 10\rangle + |10, 10, 01, 01\rangle \\ & - |10, 00, 11, 01\rangle - \sqrt{2}|10, 00, 02, 10\rangle \\ & + \sqrt{2}|01, 20, 00, 01\rangle + |01, 11, 00, 10\rangle \\ & - |01, 10, 01, 10\rangle - \sqrt{2}|01, 00, 20, 01\rangle \\ & + |01, 01, 10, 10\rangle - |01, 00, 11, 10\rangle ] \quad (\text{A7}) \end{aligned}$$

Ideally then, if one were to obtain a 1-2 coincidence or a 3-4 coincidence in the detectors at the four dual-rail modes, a successful entanglement swap would be declared and a new state  $|M_{ad}^+\rangle$  would be ascribed to the photons

in quantum memory. However with noisy detectors, one should use Lüders' rule for the POVM above to get the new state. For instance, suppose we were to detect a 1-2 coincidence in the detectors. Then, this is signified by

the POVM element

$$\begin{aligned} & F_1 \otimes F_1 \otimes F_0 \otimes F_0 \\ &= P_e^2(1 - P_e^2)^2 \Pi_0 \otimes \Pi_0 \otimes \Pi_0 \otimes \Pi_0 \\ &+ P_e^2(1 - P_e^2)(1 - A_e) \Pi_0 \otimes \Pi_0 \otimes \Pi_0 \otimes \Pi_1 + \dots \end{aligned} \quad (\text{A8})$$

and the new state for the  $a$ - $d$  system will be

$$\rho'_{ad} = \frac{1}{\text{Prob}(F_1 \otimes F_1 \otimes F_0 \otimes F_0)} \text{tr}_{bc} \left( \sqrt{F_1 \otimes F_1 \otimes F_0 \otimes F_0} |\text{swap}\rangle \langle \text{swap}| \sqrt{F_1 \otimes F_1 \otimes F_0 \otimes F_0} \right). \quad (\text{A9})$$

From here on out is just a question of brute-force calculation. At the end of it, one finds:

$$\begin{aligned} \rho'_{ad} = \frac{1}{8s_1} & \left\{ \left[ A_e^2(1 - P_e)^2 + P_e^2(1 - A_e)^2 \right] |M_{ad}^+\rangle \langle M_{ad}^+| \right. \\ & + 2A_e P_e(1 - A_e)(1 - P_e) |M_{ad}^-\rangle \langle M_{ad}^-| \\ & + P_e(1 - P_e) \left[ P_e(1 - B_e) + B_e(1 - P_e) \right] \times \\ & \left. \left( |01, 01\rangle \langle 01, 01| + |10, 10\rangle \langle 10, 10| \right) \right\}, \quad (\text{A10}) \end{aligned}$$

where,

$$s_1 = \frac{1}{8} \left[ (A_e + P_e - 2A_e P_e)^2 + P_e(1 - P_e)(B_e + P_e - 2B_e P_e) \right]. \quad (\text{A11})$$

Thus one has mostly the swap expected. But with some probability one gets an unexpected swap, and with some probability an induced classical correlation between the photons in the memory. By symmetry one has the same result for a 3-4 coincidence, and for 1-4 and 2-3 coincidences, one just interchanges the roles of  $|M_{ad}^+\rangle$  and  $|M_{ad}^-\rangle$  in this expression. We therefore have the state of an elementary link given by:

$$\begin{aligned} \rho_1 = \frac{1}{s_1} & \left[ a_1 |M^+\rangle \langle M^+| + b_1 |M^-\rangle \langle M^-| + c_1 |\psi_0\rangle \langle \psi_0| \right. \\ & \left. + d_1 |\psi_1\rangle \langle \psi_1| + d_1 |\psi_2\rangle \langle \psi_2| + c_1 |\psi_3\rangle \langle \psi_3| \right], \quad (\text{A12}) \end{aligned}$$

where  $|\psi_0\rangle = |01, 01\rangle$ ,  $|\psi_1\rangle = |01, 10\rangle$ ,  $|\psi_2\rangle = |10, 01\rangle$ ,  $|\psi_3\rangle = |10, 10\rangle$ ,  $|M^\pm\rangle = [|\psi_2\rangle \pm |\psi_1\rangle]/\sqrt{2}$ ,  $s_1 = a_1 + b_1 + 2(c_1 + d_1)$  is a normalization constant, and the coefficients  $a_1, b_1, c_1, d_1$  are given by:

$$\begin{aligned} a_1 &\equiv a_e = \frac{1}{8} \left[ P_e^2(1 - A_e)^2 + A_e^2(1 - P_e)^2 \right], \\ b_1 &\equiv b_e = \frac{1}{8} \left[ 2A_e P_e(1 - A_e)(1 - P_e) \right], \\ c_1 &\equiv c_e = \frac{1}{8} P_e(1 - P_e) \left[ P_e(1 - B_e) + B_e(1 - P_e) \right], \\ d_1 &\equiv d_e = 0, \end{aligned}$$

where  $A_e = \eta_e \lambda + P_e(1 - \eta_e \lambda)$  and  $B_e = 1 - (1 - P_e)(1 - \eta_e \lambda)^2$ .

## 2. Connections through swap stages at the quantum repeater nodes

Next we consider the case  $i \geq 2$ . The proof proceeds as follows. We first realize, by term-by-term evaluation of connecting two copies of  $\rho_1$ , that the state  $\rho_i$  never goes outside the span of  $|\psi_0\rangle, |\psi_1\rangle, |\psi_2\rangle, |\psi_3\rangle$ . It is convenient to express the state  $\rho_i$  as:

$$\begin{aligned} \rho_i = \frac{1}{s_i} & \left[ r_1^{(i)} |M^+\rangle \langle M^+| + r_2^{(i)} |M^-\rangle \langle M^-| + r_3^{(i)} |\psi_0\rangle \langle \psi_0| \right. \\ & \left. + r_4^{(i)} |\psi_1\rangle \langle \psi_1| + r_5^{(i)} |\psi_2\rangle \langle \psi_2| + r_6^{(i)} |\psi_3\rangle \langle \psi_3| \right], \quad (\text{A13}) \end{aligned}$$

where  $s_i = \sum_{l=1}^6 r_l^{(i)}$ . Then, we realize that each subsequent connection evolves the state as,

$$r_l^{(i+1)} = \sum_{j=1}^6 \sum_{k=1}^6 C_{j,k,l} r_j^{(i)} r_k^{(i)}, \quad (\text{A14})$$

with the matrix  $C$  given by (each term of which is calculated by brute-force algebra):

$$\begin{aligned} C(1, 1, :) &= [a, b, c, 0, 0, c] \\ C(1, 2, :) &= [b, a, c, 0, 0, c] \\ C(1, 3, :) &= [0, 0, a + b, 0, 2c, 0] \\ C(1, 4, :) &= [0, 0, 0, a + b, 0, 2c] \\ C(1, 5, :) &= [0, 0, 2c, 0, a + b, 0] \\ C(1, 6, :) &= [0, 0, 0, 2c, 0, a + b], \\ C(2, 1, :) &= [a, b, c, 0, 0, c] \\ C(2, 2, :) &= [b, a, c, 0, 0, c] \\ C(2, 3, :) &= [0, 0, a + b, 0, 2c, 0] \\ C(2, 4, :) &= [0, 0, 0, a + b, 0, 2c] \\ C(2, 5, :) &= [0, 0, 2c, 0, a + b, 0] \\ C(2, 6, :) &= [0, 0, 0, 2c, 0, a + b], \\ C(3, 1, :) &= [0, 0, a + b, 2c, 0, 0] \\ C(3, 2, :) &= [0, 0, a + b, 2c, 0, 0] \\ C(3, 3, :) &= [0, 0, 4c, 0, 0, 0] \\ C(3, 4, :) &= [0, 0, 0, 4c, 0, 0] \\ C(3, 5, :) &= [0, 0, 2(a + b), 0, 0, 0] \\ C(3, 6, :) &= [0, 0, 0, 2(a + b), 0, 0], \end{aligned}$$

$$\begin{aligned}
C(4, 1, :) &= [0, 0, 2c, a + b, 0, 0] \\
C(4, 2, :) &= [0, 0, 2c, a + b, 0, 0] \\
C(4, 3, :) &= [0, 0, 2(a + b), 0, 0, 0] \\
C(4, 4, :) &= [0, 0, 0, 2(a + b), 0, 0] \\
C(4, 5, :) &= [0, 0, 4c, 0, 0, 0] \\
C(4, 6, :) &= [0, 0, 0, 4c, 0, 0],
\end{aligned}$$

$$\begin{aligned}
C(5, 1, :) &= [0, 0, 0, 0, a + b, 2c] \\
C(5, 2, :) &= [0, 0, 0, 0, a + b, 2c] \\
C(5, 3, :) &= [0, 0, 0, 0, 4c, 0] \\
C(5, 4, :) &= [0, 0, 0, 0, 0, 4c] \\
C(5, 5, :) &= [0, 0, 0, 0, 2(a + b), 0] \\
C(5, 6, :) &= [0, 0, 0, 0, 0, 2(a + b)],
\end{aligned}$$

$$\begin{aligned}
C(6, 1, :) &= [0, 0, 0, 0, 2c, a + b] \\
C(6, 2, :) &= [0, 0, 0, 0, 2c, a + b] \\
C(6, 3, :) &= [0, 0, 0, 0, 2(a + b), 0] \\
C(6, 4, :) &= [0, 0, 0, 0, 0, 2(a + b)] \\
C(6, 5, :) &= [0, 0, 0, 0, 4c, 0] \\
C(6, 6, :) &= [0, 0, 0, 0, 0, 4c], \tag{A15}
\end{aligned}$$

where the “:” sign indicates all entries  $C(j, k, l)$  for  $1 \leq l \leq 6$ . The rest is just writing out  $r_i^{(i+1)}$  explicitly, and realizing that,

$$r_3^{(i)} = r_6^{(i)}, \text{ and} \tag{A16}$$

$$r_4^{(i)} = r_5^{(i)}, \tag{A17}$$

and hence the fact that we can rename the coefficients as:  $r_1^{(i)} = a_i, r_2^{(i)} = b_i, r_3^{(i)} = r_6^{(i)} = c_i$ , and  $r_4^{(i)} = r_5^{(i)} = d_i$ .

## Appendix B: Evaluating the success probabilities

It is easy to realize from the derivation of the states  $\rho_i$  that the success probability (to connect two copies of  $\rho_{i-1}$  to obtain one copy of  $\rho_i$ ) is simply given by  $P_s(i) = 4s_i$ , for  $i \geq 2$ . The probability an elementary link is successfully created is  $P_s(1) = 1 - (1 - P_{s0})^M$ , where  $P_{s0} = 4s_1$  is the probability of successful creation of an elementary link  $\rho_1$  in one of the  $M$  frequencies at the center of the elementary link, where  $s_1 = a_e + b_e + 2c_e$ . It is simple now to calculate the success probabilities  $P_s(i)$  by proving that  $s_i = s, \forall i \geq 2$ . We thus have the following proposition.

**Proposition 3** *The success probability of connecting two copies of  $\rho_{i-1}$  to produce a usable copy of  $\rho_i$ ,  $P_s(i) = 4s_i$ , where*

$$s_i = a + b + 2c \triangleq s, 2 \leq i \leq n + 1. \tag{B1}$$

**Proof.** Denoting  $x_i = a_i + b_i + c_i + d_i$ , and  $y_i = c_i + d_i$ , using Eqs. (6), (7), (8), (9), we have,

$$x_{i+1} = \frac{1}{s_i^2} [(a + b + c)(x_i^2 + y_i^2) + 2cx_iy_i], \tag{B2}$$

$$y_{i+1} = \frac{1}{s_i^2} [c(x_i - y_i)^2 + 2(a + b + 2c)x_iy_i], \tag{B3}$$

with  $s_i = x_i + y_i$  by definition. It is easy to now see that  $x_{i+1} + y_{i+1} = a + b + 2c \equiv s$ , for all  $i \in \{2, 3, \dots, n + 1\}$ . Note that  $P_s(1) = 1 - (1 - 4s_1)^M$ , with  $s_1 = a_e + b_e + 2c_e$  for the elementary link. ■

## Appendix C: Evaluating the sift probability

In this Appendix, we derive  $P_1$ , the probability that Alice and Bob both get exactly one click each, i.e., they decide to use their click outcomes for further processing to extract a key when they measure their halves of the shared entangled state  $\rho_{n+1}$ , after  $N = 2^n$  elementary links have been connected successfully.

Let us first assume Alice and Bob share the state  $\rho_i$ , and they make a measurement (in the same basis). We proceed as follows.

**Proposition 4** *Let  $P_1$  denote the probability that Alice and Bob both get exactly one click each, i.e., they decide to use their click outcomes for further processing to extract a key. It is straightforward to argue that, regardless of the value of  $i$ ,*

$$P_1 = (q_1 + q_2)^2, \tag{C1}$$

where  $q_1 = (1 - P_d)A_d$ ,  $q_2 = (1 - A_d)P_d$ , with  $A_d = \eta_d P_d + 1 - \eta_d$  are loss and noise parameters of Alice’s and Bob’s single-photon detectors.

**Proof.** This can be proven rigorously by simply evaluating  $\text{Tr}[\rho_i(M_{0101} + M_{0110} + M_{1001} + M_{1010})]$ , where  $M_{ijkl} \equiv F_i \otimes F_j \otimes F_k \otimes F_l$ , with the POVM elements of a lossy-noisy single-photon detector POVMs  $F_0$  and  $F_1$  defined above. Here we will sketch a more intuitive (but less rigorous) proof. Note that  $\rho_i \in \text{span}(|\psi_0\rangle, |\psi_1\rangle, |\psi_2\rangle, |\psi_3\rangle)$ , with  $|\psi_0\rangle = |01, 01\rangle$ ,  $|\psi_1\rangle = |01, 10\rangle$ ,  $|\psi_2\rangle = |10, 01\rangle$ ,  $|\psi_3\rangle = |10, 10\rangle$ , since  $|M^\pm\rangle = [|\psi_2\rangle \pm |\psi_1\rangle] / \sqrt{2}$ . Therefore, Alice’s and Bob’s reduced density operators always have exactly one photon in one of two modes. Let us define  $q_1 \triangleq P[\text{noflip}]$  to be the probability that a  $|01\rangle$  state is detected as “(0, 1)” by the lossy-noisy detector, where (0, 1) stands for (no-click, click). Clearly,  $q_1$  is also the probability that  $|10\rangle$  is detected as “(1, 0)”. In order for “no flip” to happen, no dark click should appear in the mode in the vacuum state (this happens with probability  $P_d$ ), and that the photon in the other mode should either be detected by the lossy detector (happens with probability  $1 - \eta_d$ , in which case it does not matter whether or not a dark click appears), or the photon does not get detected, and a dark click appears (which happens with probability  $\eta_d P_d$ ). Therefore,  $q_1 = (1 - P_d)A_d$ ,

with  $A_d = \eta_d P_d + 1 - \eta_d$ . Similarly, we define  $q_2 \triangleq P[\text{flip}]$  to be the probability that  $|01\rangle$  is detected as “(1,0)” (or,  $|10\rangle$  is detected as “(0,1)”). For a “flip” event to happen, a dark click should appear in the vacuum mode (probability  $P_d$ ), and the photon containing mode should not be detected *and* a dark click must not appear (happens with probability,  $\eta_d(1 - P_d)$ ). Therefore,  $q_2 = (\eta_d(1 - P_d))P_d = (1 - A_d)P_d$ . Clearly,  $q_1 + q_2$  need not add up to 1 in general, since the detectors may output “(0,0)” or “(1,1)” outcomes, which are not used by Alice and Bob. Therefore  $(q_1 + q_2)^2$  is the probability that Alice and Bob obtain a *usable* detection outcome, i.e., both of them collectively obtain one of the four outcomes: (0, 1; 0, 1), (0, 1; 1, 0), (1, 0; 0, 1), (1, 0; 1, 0). This is true regardless of the actual fraction of  $|10\rangle$  and  $|01\rangle$  in Alice’s and Bob’s states. Hence,  $P_1 = (q_1 + q_2)^2$ . ■

#### Appendix D: The QBER and secret key rate

In this Appendix, we will evaluate the explicit formula for  $Q_i$ , the quantum bit-error rate (QBER), which is the probability that Alice and Bob obtain a mismatched raw key bit, despite the fact that they make measurements in the same bases on a successfully-created copy of  $\rho_i$ , *and* that they both get exactly single-clicks (on the two modes of their respective qubits). The first step in doing so is to solve for the quantum state  $\rho_i$  more explicitly than what the recursions in Proposition 2 give us.

##### 1. Explicit solution for the quantum state, $\rho_i$

Recall that we proved above that  $s_i = a + b + 2c \triangleq s$ ,  $2 \leq i \leq n + 1$ , by defining  $x_i = a_i + b_i + c_i + d_i$ , and  $y_i = c_i + d_i$ , and using Eqs. (6), (7), (8), (9), to obtain  $x_{i+1} + y_{i+1} = a + b + 2c \equiv s$ , for all  $i \in \{2, 3, \dots, n + 1\}$ , and that  $s_1 = a_e + b_e + 2c_e$  for the elementary link. Let us now proceed to calculate the coefficients  $a_i$ ,  $b_i$ ,  $c_i$  and  $d_i$ , all explicitly as a function of  $i$ ,  $1 \leq i \leq n + 1$ , and the system’s loss and noise parameters.

**Proposition 5**  $a_i + b_i \equiv z_i$  is given by,

$$z_i = \nu \left( \frac{z_1}{\nu} \times \frac{s}{s_1} \right)^{2^{i-1}}, \quad i \geq 2, \quad (\text{D1})$$

where  $z_1 = a_e + b_e$ ,  $s_1 = a_e + b_e + 2c_e$ ,  $\nu = s^2/(a + b)$ , and  $s \triangleq s_i$ , for  $i \geq 2$ .

**Proof.** The proof follows by realizing that with the definitions in Eqs. (B2) and (B3),  $x_i - y_i = a_i + b_i$ , and,

$$x_{i+1} - y_{i+1} = \frac{1}{s_i^2} (a + b)(x_i - y_i)^2. \quad (\text{D2})$$

**Remark 6** Note that since  $x_i + y_i = s_i$ , and  $x_i - y_i = z_i$ , we have,

$$y_i = c_i + d_i = \frac{1}{2} \left[ s_i - \nu \left( \frac{s z_1}{s_1 \nu} \right)^{2^{i-1}} \right]. \quad (\text{D3})$$

As we will see in the next subsection, the error probability  $Q_i$  depends only on  $2c_i/s_i$ —the fractional probability of the classical correlations when two copies of  $\rho_{i-1}$  are connected. Note that  $(a_i + b_i)$  is the sum fractional probability of the Bell states  $|M^+\rangle$  ( $a_i$ ) and  $|M^-\rangle$  ( $b_i$ ) when two copies of  $\rho_{i-1}$  are connected, and  $s_i = (a_i + b_i) + 2c_i$ . Since we already have  $c_i + d_i$  explicitly available, let us calculate  $c_i - d_i \equiv u_i$ .

**Proposition 7** The difference  $c_i - d_i \equiv u_i$  can be found as the solution to the following quadratic difference equation,

$$w_{i+1} = w_r + 2(1 - 2w_r)w_i(1 - w_i), \quad (\text{D4})$$

where  $w_i \triangleq u_i/z_i$ ,  $w_r = c/(a + b)$ , and  $w_1 = c_e/(a_e + b_e)$ .

**Proof.** The proof follows from simply writing down  $c_{i+1} - d_{i+1}$  using Eqs. (8) and (9), substituting  $w_i = u_i/z_i$ , and simplifying. ■

**Remark 8** The difference equation equation (D4) reduces to the famous Logistic Map, when  $w_r = 0$ . The solution to the logistic map  $w_{i+1} = R w_i(1 - w_i)$ ,  $w_i \in (0, 1)$ , is in general chaotic, but for  $R = 2$  (which is exactly what (D4) reduces to when  $w_r = 0$ ) was found exactly by Ernst Schröder in 1870, as:

$$w_i = \frac{1}{2} \left[ 1 - (1 - 2w_1)^{2^{i-1}} \right]. \quad (\text{D5})$$

**Theorem 9** The quadratic difference equation,  $w_{i+1} = w_r + 2(1 - 2w_r)w_i(1 - w_i)$ , which is a variant of the logistic map  $w_{i+1} = 2w_i(1 - w_i)$  with  $R = 2$ , can be exactly solved, and the solution is given by:

$$w_i = \frac{1}{2} \left[ 1 - \frac{1}{\beta} [\beta(1 - 2w_1)]^{2^{i-1}} \right], \quad (\text{D6})$$

where  $\beta = 1 - 2w_r$ . This correctly reduces to (E2) when  $w_r = 0$ .

**Proof.** See next Section for the proof. ■

Next, we find  $c_i$ . We add the following two expressions:

$$c_i + d_i = (s_i - z_i)/2, \quad \text{and} \quad (\text{D7})$$

$$c_i - d_i = u_i = \frac{z_i}{2} \left[ 1 - \frac{1}{\beta} [\beta(1 - 2w_1)]^{2^{i-1}} \right], \quad (\text{D8})$$

and divide by 2, to obtain:

$$c_i = \frac{s_i}{4} \left[ 1 - \frac{z_i}{\beta s_i} [\beta(1 - 2w_1)]^{2^{i-1}} \right]. \quad (\text{D9})$$

At this point, since we have  $c_i$ , it is sufficient to calculate  $Q_i$  (see next subsection). However, let us go ahead

and evaluate  $a_i$  and  $b_i$  as well, so that we have a complete characterization of the quantum state  $\rho_i$ , which can be used to calculate other quantities of interest, such as the fidelity, entanglement of formation, etc.

Since we already have  $a_i + b_i = z_i$  from Proposition 5, we need to calculate  $a_i - b_i$ .

**Proposition 10**  $a_i - b_i \equiv v_i$  is given by the following recursion,

$$v_i = \frac{1}{s_i^2}(a - b)z_i v_i, \quad (\text{D10})$$

which can be solved to obtain:

$$v_i = \left(\frac{a - b}{a + b}\right)^{i-1} \left(\frac{a_e - b_e}{a_e + b_e}\right) z_i, \quad (\text{D11})$$

where  $z_i$  is given by Eq. (D1).

**Proof.** The proof follows simply by subtracting the expressions for  $b_{i+1}$  from that of  $a_{i+1}$ , given in Proposition 2, and simplifying. ■

With that, we finally have the state  $\rho_i$  as,

$$\rho_i = \frac{1}{s_i} [a_i |M^+\rangle\langle M^+| + b_i |M^-\rangle\langle M^-| + c_i |\psi_0\rangle\langle\psi_0| + d_i |\psi_1\rangle\langle\psi_1| + d_i |\psi_2\rangle\langle\psi_2| + c_i |\psi_3\rangle\langle\psi_3|], \quad (\text{D12})$$

where  $|\psi_0\rangle = |01, 01\rangle$ ,  $|\psi_1\rangle = |01, 10\rangle$ ,  $|\psi_2\rangle = |10, 01\rangle$ ,  $|\psi_3\rangle = |10, 10\rangle$ ,  $|M^\pm\rangle = [|\psi_2\rangle \pm |\psi_1\rangle]/\sqrt{2}$ ,  $s_i = a_i + b_i + 2(c_i + d_i)$ , and the coefficients given as:

$$\begin{aligned} a_i &= \frac{1}{2} \left[ 1 + \left(\frac{a - b}{a + b}\right)^{i-1} \left(\frac{a_e - b_e}{a_e + b_e}\right) \right] z_i, \\ b_i &= \frac{1}{2} \left[ 1 - \left(\frac{a - b}{a + b}\right)^{i-1} \left(\frac{a_e - b_e}{a_e + b_e}\right) \right] z_i, \\ c_i &= \frac{s_i}{4} \left[ 1 - \frac{z_i}{s_i(1 - 2w_r)} [(1 - 2w_r)(1 - 2w_1)]^{2^{i-1}} \right], \\ d_i &= \frac{s_i}{4} - \frac{z_i}{2} \left[ 1 - \frac{1}{2(1 - 2w_r)} [(1 - 2w_r)(1 - 2w_1)]^{2^{i-1}} \right], \end{aligned}$$

with  $w_i = c_e/(a_e + b_e)$ ,  $w_r = c/(a + b)$ ,  $s_1 = a_e + b_e + 2c_e$ ,  $s_i = s = a + b + 2c$ ,  $2 \leq i \leq n + 1$ , and  $z_i$  given by,

$$z_i = \left(\frac{s^2}{a + b}\right) \left(\frac{1}{(1 + 2w_1)(1 + 2w_r)}\right)^{2^{i-1}}, \quad i \geq 2, \quad (\text{D13})$$

with  $z_1 = a_e + b_e$ . The expressions for  $a_i$ ,  $b_i$ ,  $c_i$ , and  $d_i$  correctly reduce to  $a_e$ ,  $b_e$ ,  $c_e$ , and 0, respectively, for  $i = 1$ . As an example calculation, the fidelity of  $\rho_i$  (with respect to  $|M^+\rangle$ ),  $F_i = \sqrt{\langle M^+ | \rho_i | M^+ \rangle}$  is given by,  $F_i = \sqrt{(a_i + d_i)/s_i}$ .

## 2. Evaluating the formula for QBER

**Proposition 11** Assume that Alice and Bob have made a measurement on  $\rho_i$ ,  $i \in \{1, \dots, n + 1\}$ . Conditioned on

the fact that they get exactly one click each on their qubits (which happens with probability  $P_1$ , as proven in Proposition 4), the probability  $Q_i$ , that they obtain a mismatched bit (a bit error) is given by,

$$Q_i = \frac{1}{2} \left[ 1 - \frac{t_d}{t_r} (t_r t_e)^{2^{i-1}} \right], \quad 1 \leq i \leq n + 1, \quad (\text{D14})$$

where  $t_e = (a_e + b_e - 2c_e)/(a_e + b_e + 2c_e)$ ,  $t_r = (a + b - 2c)/(a + b + 2c)$ , and  $t_d = ((q_1 - q_2)/(q_1 + q_2))^2$  are loss-noise parameters of detectors in the elementary links, memory nodes, and Alice-Bob, respectively.

**Proof.** The first step is to show that  $Q_i$  can be expressed as follows:

$$Q_i = \frac{1}{2} [1 - t_d(1 - 2\zeta_i)], \quad (\text{D15})$$

where  $\zeta_i = 2c_i/s_i$ ,  $t_d = ((q_1 - q_2)/(q_1 + q_2))^2$ . Since we have shown that  $s_i = s = a + b + 2c$ ,  $i \geq 2$ , and  $s_1 = a_e + b_e + 2c_e$ , we only need to solve for  $c_i$ , in order to evaluate  $Q_i$ . In order to prove (D15), we can evaluate  $Q_i = \text{Tr}[\rho_i(M_{0101} + M_{1010})]/\text{Tr}[\rho_i(M_{0101} + M_{0110} + M_{1001} + M_{1010})]$ , where the denominator is  $P_1$ . It is easy to argue (D15) informally as follows. We first note that  $\rho_i$  is of the form,

$$\rho_i = r_1 |M^+\rangle\langle M^+| + r_2 |M^-\rangle\langle M^-| + r_3 |\psi_0\rangle\langle\psi_0| + r_4 |\psi_1\rangle\langle\psi_1| + r_5 |\psi_2\rangle\langle\psi_2| + r_6 |\psi_3\rangle\langle\psi_3|, \quad (\text{D16})$$

with  $\sum_{i=1}^6 r_i = 1$ .  $Q_i = (Q_1 + Q_2)/P_1$ , where

$$Q_1 = q_1^2 r_3 + q_1 q_2 \left[ r_4 + \frac{1}{2}(r_1 + r_2) + r_5 + \frac{1}{2}(r_1 + r_2) \right] + q_2^2 r_6, \quad \text{and} \quad (\text{D17})$$

$$Q_2 = q_2^2 r_3 + q_1 q_2 \left[ r_4 + \frac{1}{2}(r_1 + r_2) + r_5 + \frac{1}{2}(r_1 + r_2) \right] + q_1^2 r_6, \quad (\text{D18})$$

since the relative contributions of  $|\psi_0\rangle, |\psi_1\rangle, |\psi_2\rangle, |\psi_3\rangle$  in  $\rho_i$  are  $r_3, r_4 + (r_1 + r_2)/2, r_5 + (r_1 + r_2)/2$ , and  $r_6$  respectively. Simplifying everything, and substituting  $P_1 = (q_1 + q_2)^2$ , we get,

$$Q_i = \left(\frac{q_1 - q_2}{q_1 + q_2}\right)^2 (r_3 + r_6) + \frac{2q_1 q_2}{(q_1 + q_2)^2}. \quad (\text{D19})$$

Now substituting  $r_3 = r_6 = c_i/s_i$ , defining  $\zeta_i = 2c_i/s_i$ , and  $t_d = ((q_1 - q_2)/(q_1 + q_2))^2$ , Eq. D15 follows.

We now divide  $2c_i$  (from Eq. (D9)) by  $s_i$  to obtain,

$$\zeta_i = \frac{2c_i}{s_i} = \frac{1}{2} \left[ 1 - \frac{z_i}{\beta s_i} [\beta(1 - 2w_1)]^{2^{i-1}} \right]. \quad (\text{D20})$$

Substituting the expression for  $z_i$  above, and realizing that  $s_i = s$ ,  $i \geq 2$ , and  $s_1 = a_e + b_e + 2c_e$ , it is easy to obtain the expression for  $Q_i$  in Eq. D14 after some

algebraic manipulations. The  $i = 1$  case must be handled separately (since  $s_1 \neq s_i, i \geq 2$ ), but the final expression in Eq. D14 is valid for all  $i = 1, 2, \dots, n + 1$ . ■

The following corollary is an interesting consequence of Eq. D14:

**Corollary 12** *The following law for error propagation holds through the successive connections of elementary links:*

$$(1 - 2Q_{i+1}) = \frac{t_r}{t_d}(1 - 2Q_i)^2, 1 \leq i \leq n. \quad (\text{D21})$$

*An interesting thing to note about the error propagation is the constant  $t_r = (1 - 2w_r)/(1 + 2w_r)$ , which is a function of the parameter  $2w_r = 2c/(a + b)$ . We saw that when two pure bell states are ‘connected’ by a linear-optic BSM with lossy-noisy detectors,  $2c$  is the fractional probability that spills over into classical correlations (the nonentangled part), and  $a + b$  is the fractional probability that goes into one of two entangled bell states.*

Putting everything together, we finally have an expression for the secret-key rate,

$$R = \frac{P_1 P_{\text{succ}} R_2(Q_{n+1})}{2T_q} \text{ secret-key bits/sec}, \quad (\text{D22})$$

where  $P_{\text{succ}} = [4s(1 - (1 - 4s_1)^M)]^{2^n} / 4s$ ,  $P_1 = (q_1 + q_2)^2$ , and  $Q_{n+1} = \left[1 - \frac{t_d}{t_r}(t_r t_e)^{2^n}\right] / 2$ , are all defined in terms of the detector loss and noise parameters, and the total number of elementary links  $N = 2^n$ .

## Appendix E: Solution of the modified logistic map

In this section, we prove the following new variation of the logistic map, whose solutions are known to have chaotic behavior in general.

**Theorem 13** *The quadratic difference equation,  $w_{i+1} = w_r + 2(1 - 2w_r)w_i(1 - w_i)$ , which is a variant of the*

*logistic map  $w_{i+1} = 2w_i(1 - w_i)$  with  $R = 2$ , can be exactly solved, and the solution is given by:*

$$w_i = \frac{1}{2} \left[ 1 - \frac{1}{\beta} [\beta(1 - 2w_1)]^{2^{i-1}} \right], i \geq 1, \quad (\text{E1})$$

where  $\beta = 1 - 2w_r$ , and the initial value  $w_1$  specified.

**Proof.** We start with the solution to the standard logistic map with  $R = 2$ , i.e., with  $w_r = 0$ . The solution is given by:

$$w_i = \frac{1}{2} \left[ 1 - (1 - 2w_1)^{2^{i-1}} \right]. \quad (\text{E2})$$

We use the ansatz that the modified map has the solution of the form

$$w_i = \frac{1}{2} \left[ 1 - (1 - 2w_1)^{2^{i-1} + \xi_i} \right]. \quad (\text{E3})$$

Inserting this into the difference equation, we get

$$\frac{1}{2} \left[ 1 - (1 - 2w_1)^{2^{i+\xi_{i+1}}} \right] = w_r + \frac{(1 - 2w_r)}{2} \left[ 1 - (1 - 2w_1)^{2^{i+\xi_i}} \right]. \quad (\text{E4})$$

Letting  $y_i = (1 - 2w_1)^{2^{i+\xi_i}}$  and  $a = 1 - 2w_r$ , we obtain

$$y_{i+1} = a^2 y_i^2, \quad (\text{E5})$$

which can be solved to obtain

$$y_i = \frac{1}{a^2} (a^2 y_1)^{2^{i-1}}, i \geq 1, \quad (\text{E6})$$

Using this to solve for  $\xi_i$ , we get

$$\xi_i = i - \log_2 \left[ \frac{2^i \log_2(a(1 - 2w_1)) - \log_2(a^2)}{\log_2(1 - 2w_1)} \right]. \quad (\text{E7})$$

Finally, inserting the expression for  $\xi_i$  into the ansatz, we obtain the following expression for  $w_i$ .

$$w_i = \frac{1}{2} \left[ 1 - \frac{1}{a} (a(1 - 2w_1))^{2^{i-1}} \right], i \geq 1. \quad (\text{E8})$$

■